Research Square

Preprints are preliminary reports that have not undergone peer review.
They should not be considered conclusive, used to inform clinical practice,
or referenced by the media as validated information.

Heavy metals and salinity gradients in the Shatt Al-Arab outlet, northwestern Arabian Gulf

Asmaa A. Al-Halfy
University of Basrah
Maher M Mahdi
University of Basrah
Ghadeer K. Jalal
University of Basrah
Hussein B. Ghalib
hussein.ghalib@uobasrah.edu.iq
University of Basrah

Research Article

Keywords: Shatt Al-Arab, estuarine mixing, dissolved heavy metals, salinity normalisation, Sentinel-2, Arabian Gulf

Posted Date: November 17th, 2026

DOI: https://doi.org/10.21203/rs.3.rs-11456072/v1

License: This work is licensed under a Creative Commons Attribution 4.0 International License.
Read Full License

Additional Declarations: Competing interest reported. Hussein B. Ghalib is an Editorial Board Member of Discover Geoscience and confirms that he was not involved in the handling or decision-making of this manuscript. The remaining authors declare that they have no competing interests.

Heavy metals and salinity gradients in the Shatt Al-Arab outlet, northwestern Arabian Gulf

Asmaa A. Al-Halfy[1], Maher M. Mahdi[1] , Ghadeer K. Jalal[2, **], Hussein B. Ghalaib[1, *]

[1] Department of Geology, College of Science, University of Basrah, Basrah, Iraq

[2] Department of Science, Open Educational College, Basrah, Iraq

* Corresponding author: Hussein.ghalib@uobasrah.edu.iq; ghadeergeo90@gmail.com

Abstract

The Shatt Al-Arab outlet at Al-Faw is the main freshwater–seawater mixing zone of the northwestern Arabian Gulf, yet the behaviour of dissolved heavy metals along its salinity gradient is poorly documented. Field measurements at 11 sites, flame atomic absorption analyses of dissolved Zn, Cu, Pb, Fe, Mn and Cd, metal–salinity regression, salinity normalisation, principal component analysis, spatial interpolation and Sentinel-2 water and turbidity indices were combined. Salinity increased from 15.9 psu in the lower Shatt Al-Arab channel to 33.1 psu in the Gulf-facing sector, and dissolved oxygen was low (1.1–4.7 mg L^{-1}). Mean concentrations followed the order Fe (1.640 mg L^{-1}) > Pb (0.822) > Cd (0.415) > Zn (0.177) > Mn (0.138) > Cu (0.088), and Cd, Pb, Cu and Zn exceeded US EPA acute saltwater criteria at all sites. Every metal increased linearly with salinity (R^2 = 0.83–0.98), and one salinity-related component explained 75.3% of the variance. After normalisation to salinity, Cu was spatially uniform (coefficient of variation 4%), whereas Pb, Fe, Mn and Cd were depleted by 13–23% in the low-salinity channel, consistent with removal during estuarine mixing, and enriched by 15–27% along the northwestern port breakwater, indicating a local source. Because salt-matrix interference in direct flame analysis scales with salinity, normalisation also helps to separate genuine spatial signals from analytical bias. The port sector is identified as a monitoring priority, and salinity-normalised metal data are recommended for estuarine assessments in the region.

Keywords Shatt Al-Arab; estuarine mixing; dissolved heavy metals; salinity normalisation; Sentinel-2; Arabian Gulf

1 Introduction

Estuaries act as filters between rivers and the sea. As river water mixes with seawater, changes in ionic strength, pH, redox conditions and particle load can remove dissolved metals by flocculation and adsorption or release them from suspended particles by desorption and complexation [1, 2]. Plotting dissolved concentrations against salinity is the classical way to identify these processes: a linear relationship indicates conservative mixing between end-members, whereas systematic departures indicate removal or addition within the estuary [1, 3]. Iron and manganese are typically removed at low salinity by the flocculation of colloidal oxyhydroxides and humic material [2], while cadmium is commonly released from particles at higher salinity through complexation with chloride [4, 5]. Climate-driven changes in river discharge, temperature, oxygen and pH can modify these processes and therefore the fate and toxicity of metals in coastal waters [6–8].

The Arabian Gulf is a shallow, semi-enclosed marginal sea in which evaporation greatly exceeds precipitation and river inflow, producing salinities among the highest of any open water body [9]. Its northwestern corner is the only part of the Gulf that receives substantial riverine input, delivered mainly by the Shatt Al-Arab, and these freshwater shapes salinity, nutrient supply and productivity across the northwestern Gulf [10, 11]. The Gulf as a whole is regarded as one of the most heavily impacted marine regions in the world, owing to oil and gas production, shipping, desalination, coastal development and rising temperatures [12–14].

The Shatt Al-Arab outlet at Al-Faw, Iraq's only direct connection to the sea, has changed markedly over recent decades. Declining Tigris–Euphrates discharge, caused by upstream impoundment, irrigation demand and drought, has allowed seawater to intrude progressively further upstream, raising the salinity of the river and of the water supplied to Basrah [15–18], and discharge to the Gulf rarely exceeded 80 m^3 s^{-1} in the seasons preceding the extreme rainfall of 2018–2019 [11]. Iraq is highly exposed to rising temperatures, erratic rainfall and increasing evaporation [19, 20], and air temperatures over the Gulf show a significant warming trend [21, 22]. Basrah Governorate also hosts some of the largest oilfields in the region [23, 24], soils across the governorate contain elevated hydrocarbons and heavy metals [25–28], and the coastal zone carries a legacy of oil, combustion products and military debris from the conflicts of 1980–1988, 1991 and 2003 [29–32]. The construction of the Grand Faw Port has added large-scale dredging and shipping to these pressures.

Earlier studies have reported dissolved Pb, Cd, Zn and other metals in the Shatt Al-Arab River and adjacent Iraqi marine waters [33–37]; in the river, metal levels were found to depend on inflow from the Tigris, marine salt from the Gulf, oil-related emissions and the tide [33, 34], and elevated mercury has been documented in estuarine sediments along the neighbouring Khuzestan coast [38]. However, these studies mainly reported concentrations at individual stations and compared them with drinking-water guidelines; to our knowledge, none has examined how dissolved metals vary along the salinity gradient of the outlet or separated the effect of dilution from that of local sources. Satellite indices of water extent and turbidity, which can help interpret such gradients, also remain underused for the Iraqi coast [39–41].

This study therefore aimed to: (i) describe the salinity gradient and associated physicochemical conditions in the Shatt Al-Arab outlet; (ii) quantify dissolved Zn, Cu, Pb, Fe, Mn and Cd and evaluate them against marine water-quality criteria; (iii) characterise metal behaviour along the salinity gradient using metal–salinity regression and salinity normalisation; (iv) identify areas of local enrichment by combining these results with spatial interpolation and Sentinel-2-derived indices; and (v) place the findings in the context of the 2014–2024 hydroclimatic record.

2 Materials and methods

2.1 Study area

The study area lies in the far south of Basrah Governorate, between 29.82° and 29.97° N and 48.41° and 48.64° E, and covers the lower Shatt Al-Arab channel at Al-Faw, its mouth and the adjacent Gulf waters along the Al-Faw port breakwater towards Khor Abdullah (Fig. 1). The climate is hot and arid, with very low and irregular winter rainfall, and a semidiurnal, meso- to macrotidal regime drives strong mixing between river and Gulf waters [9, 16]. The coast is dominated by low-lying tidal flats and is being rapidly modified by port infrastructure, including the breakwater and basin of the Grand Faw Port (Fig. 1).

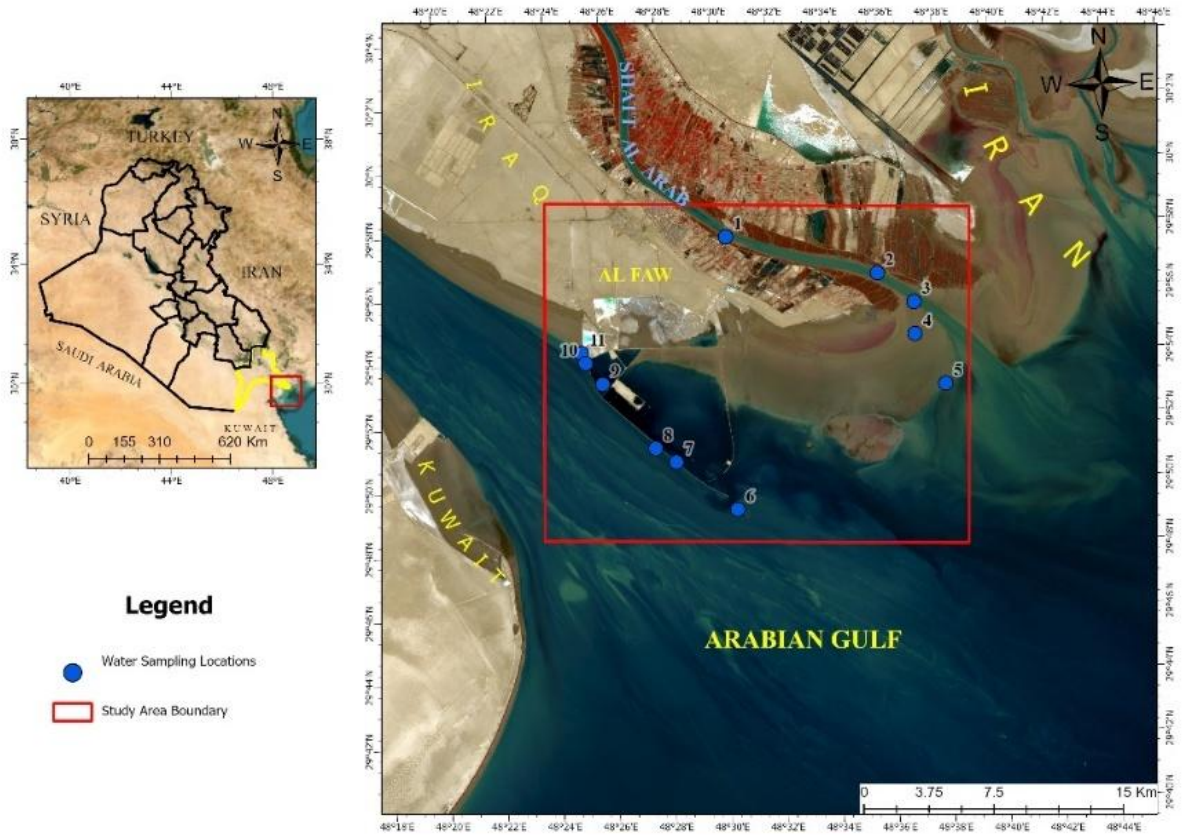


Fig. 1 Location of the study area and the 11 water sampling sites in the Shatt Al-Arab outlet, northwestern Arabian Gulf, Iraq.

2.2 Sampling and field measurements

Water samples were collected from 11 sites (Table 1) during a single marine field campaign in May 2024. Sampling depths ranged from 2 to 5 m below the water surface. The sampling locations were recorded using a handheld GPS and plotted on a georeferenced base map in ArcGIS Pro. According to their positions along the estuary–sea continuum (Fig. 1), the sites were grouped into four sectors: (A) the lower Shatt Al-Arab channel (sites 1–3); (B) the outer estuary and river mouth (sites 4–5); (C) the southern part of the Al-Faw port breakwater facing the Gulf (sites 6–8); and (D) the northwestern end of the breakwater towards Khor Abdullah (sites 9–11).

Water temperature, pH, electrical conductivity (EC), salinity, and dissolved oxygen (DO) were measured in situ using calibrated portable meters. Samples were stored in pre-cleaned polyethylene bottles at 4 °C and transported to the Marine Science Center laboratory for analysis. Samples intended for metal analysis were filtered through 0.45 µm membrane filters

and acidified with nitric acid (HNO_3) to a pH below 2. Metal concentrations were determined using a PG-990 atomic absorption spectrophotometer (AAS).

Table 1 Sampling sites, sectors and geographic coordinates (WGS 84)

Site	Sector	Latitude (°N)	Longitude (°E)
1	A – Lower channel	29.9632	48.5063
2	A – Lower channel	29.9420	48.5964
3	A – Lower channel	29.9264	48.6179
4	B – Outer estuary	29.9097	48.6179
5	B – Outer estuary	29.8834	48.6353
6	C – Southern breakwater	29.8209	48.5087
7	C – Southern breakwater	29.8465	48.4729
8	C – Southern breakwater	29.8539	48.4609
9	D – Northwestern breakwater	29.9046	48.4182
10	D – Northwestern breakwater	29.8993	48.4204
11	D – Northwestern breakwater	≈29.905 [a]	≈48.418 [a]

[a] Approximate position read from Fig. 1. The coordinates given for site 11 in the original data (29.9647° N, 48.5057° E, and 29°57′49″ N, 48°28′59″ E) are mutually inconsistent and disagree with the map; they must be verified by the authors.

2.3 Laboratory analyses and data quality

Dissolved Zn, Cu, Pb, Fe, Mn, and Cd were determined by flame atomic absorption spectrometry (PG Instruments AA-990) following Standard Methods [42]. Total dissolved solids (TDS) were estimated from electrical conductivity (EC) using a conversion factor of 640, according to the following equation:

$$\text{TDS (mg L}^{-1}) = 640 \times \text{EC (mS cm}^{-1})$$

Major ions (Ca^{2+}, Mg^{2+}, Na^{+}, K^{+}, Cl^{-}, SO_4^{2-}, HCO_3^{-} and CO_3^{2-}) were also determined. Their analytical consistency was evaluated with the charge-balance error (CBE), calculated from concentrations in meq L^{-1}:

$$CBE = \frac{\Sigma cations - \Sigma anions}{\Sigma cations + \Sigma anions} \times 100 \quad (1)$$

The CBE values ranged from −6.8 to −42.9%, and no sample met the commonly accepted criterion of ±5%; molar Na^{+}/Cl^{-} ratios (0.18–0.38) were also far below the seawater value of 0.86 [43]. Because the samples were no longer available for re-analysis, the major-ion data were excluded from interpretation. They are reported, with these quality indicators, in ESM 1 for transparency.

2.4 Remote sensing and spatial interpolation

A cloud-free Sentinel-2 MSI Level-2A scene acquisition date and tile ID was used to derive two indices at 10 m resolution. The Normalized Difference Water Index (NDWI) was calculated after McFeeters [39]:

$$NDWI = \frac{B3-B8}{B3+B8} \quad (2)$$

where B3 and B8 are the green and near-infrared bands, respectively. A relative turbidity index (TI) was calculated from the red (B4) and blue (B2) bands, exploiting the increase in red reflectance with suspended particulate matter in turbid coastal waters [40, 41]:

$$TI = \frac{B4-B2}{B4+B2} \quad (3)$$

TI is used as a qualitative indicator of relative suspended-sediment load; it was not calibrated against in situ turbidity measurements. Spatial distribution maps of the measured variables were generated in ArcGIS Pro by inverse distance weighting (IDW) [44]. Given the small number of sites and the complex coastline, the interpolated surfaces are interpreted only as indicators of broad spatial gradients.

2.5 Data analysis

Descriptive statistics (minimum, maximum, mean, standard deviation and coefficient of variation, CV) were computed for all variables. Relationships among variables were evaluated with Spearman's rank correlation coefficient (ρ; significance at $p < 0.05$). Metal behaviour along the mixing gradient was examined with metal–salinity diagrams [1, 3]: each metal was regressed against salinity by ordinary least squares, and the deviation of each site from the regression line was expressed as a percentage of the predicted value. To remove the effect of dilution and of any analytical bias that scales with salt content, salinity-normalised concentrations were calculated as the ratio of metal concentration (μg L^{-1}) to salinity (psu); their spatial heterogeneity was described by the CV and compared among sectors. Principal component analysis (PCA) was performed on the correlation matrix of 11 standardised variables (Zn, Cu, Pb, Fe, Mn, Cd, EC, salinity, DO, pH and water temperature), retaining components with eigenvalues greater than 1. Metal–salinity analyses and PCA used the ten sites with complete field records (sites 1–10). Because of the small number of sites, sector comparisons are descriptive and the PCA is exploratory. Analyses were carried out in Python (SciPy and NumPy).

2.6 Assessment criteria

Because the study area is not a drinking-water source, metal concentrations were evaluated primarily against the US EPA national recommended aquatic life criteria for saltwater: the criterion maximum concentration (CMC, acute) and the criterion continuous concentration (CCC, chronic) [45]. Exceedance factors (EF) were calculated as the ratio of measured concentration to criterion. WHO drinking-water guideline values [46] are reported for reference only, to allow comparison with earlier regional studies.

2.7 Hydroclimatic data

Annual mean air temperature and mean daily precipitation for 2014–2024 were obtained for the Al-Faw station from the Agricultural Meteorology Centre, Ministry of Agriculture, Basra Governorate, Iraq. Please confirm the precipitation unit: values of 0.03–0.89 are consistent with mean daily rates (mm d^{-1}). Monotonic trends were evaluated using the Mann–Kendall test and Sen's slope estimator [47, 48].

3 Results

3.1 Salinity gradient and physicochemical conditions

Physicochemical parameters are summarised in Table 2 and given for each site in ESM 1. Salinity ranged from 15.89 to 33.13 psu (mean 25.96 ± 7.04 psu) and EC from 26.7 to 52.5 mS cm^{-1} (mean 44.1 ± 9.3 mS cm^{-1}); the two were closely related (R^2 = 0.84). Salinity increased from the lower Shatt Al-Arab channel (sector A: 16.3–27.4 psu) to the outer estuary (sector B: 32.4 psu at both sites) and the southern breakwater (sector C: 28.5–33.1 psu), whereas the northwestern breakwater sites had low salinities (sector D: 15.9–19.4 psu). The IDW maps reproduce this gradient, with the lowest EC, salinity and TDS along the river channel and in the northwest and the highest values in the south-central and eastern parts of the study area (Fig. 2). Water temperature varied within a narrow range (28.0–30.0 °C) and pH was slightly alkaline (7.29–7.99). Dissolved oxygen was low throughout (1.10–4.70 mg L^{-1}; mean 2.69 ± 1.14 mg L^{-1}); eight of ten sites had DO < 4 mg L^{-1}, and three (sites 1, 2 and 9) were below the commonly used hypoxia threshold of 2 mg L^{-1}. DO increased with EC (ρ = 0.85).

Table 2 Descriptive statistics of physicochemical parameters in the Shatt Al-Arab outlet (n = 10)

Parameter	Unit	Min	Max	Mean	SD	CV (%)
Water temperature	°C	28.0	30.0	29.0	0.8	2.8
pH	–	7.29	7.99	7.79	0.22	2.9
EC	mS cm^{-1}	26.7	52.5	44.1	9.3	21.1
TDS [a]	mg L^{-1}	17,088	33,600	28,218	5,959	21.1
Salinity	psu	15.89	33.13	25.96	7.04	27.1
DO	mg L^{-1}	1.10	4.70	2.69	1.14	42.3

[a] Estimated from EC (TDS = 0.64 × EC). Site 11 lacks field measurements (see ESM 1).

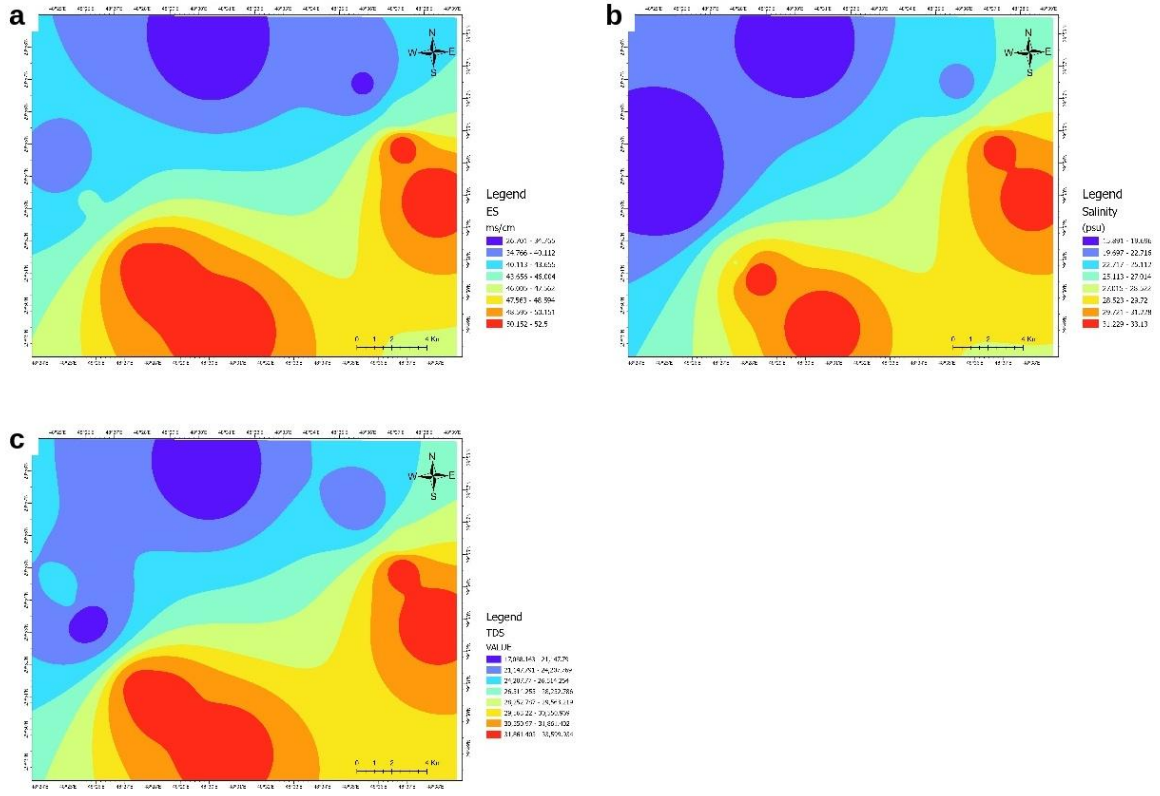


Fig. 2 IDW interpolation maps of (a) electrical conductivity (mS cm^{-1}), (b) salinity (psu) and (c) total dissolved solids (mg L^{-1}) .

3.2 Dissolved metal concentrations and exceedance of criteria

Mean dissolved metal concentrations decreased in the order Fe (1.640 ± 0.474 mg L^{-1}) > Pb (0.822 ± 0.220) > Cd (0.415 ± 0.100) > Zn (0.177 ± 0.031) > Mn (0.138 ± 0.054) > Cu (0.088 ± 0.024 mg L^{-1}) (Table 3; Fig. 3). The lowest concentrations of all metals occurred at site 1 in the river channel and the highest at sites 4–8. Lead (1.005 mg L^{-1}) and Fe (2.016 mg L^{-1})

reached identical maximum values at four to five sites in sectors B and C, a pattern considered in Sect. 4.4.

All Cd, Pb, Cu and Zn concentrations exceeded the US EPA acute saltwater criteria, by factors of 7.1–15.3 for Cd, 1.9–4.8 for Pb, 12.1–24.4 for Cu and 1.4–2.4 for Zn, and exceeded the chronic criteria by factors of 30–64, 50–124, 19–38 and 1.6–2.7, respectively (Table 4). For reference, Pb and Cd also exceeded the WHO drinking-water guideline values by factors of 40–101 and 78–169, whereas Zn and Cu were below them.

Table 3 Dissolved heavy metal concentrations (mg L^{-1}, n = 11) and assessment criteria

Metal	Range	Mean ± SD	WHO [a]	EPA CMC [b]	EPA CCC [b]
Fe	0.756–2.079	1.640 ± 0.474	– [d]	–	–
Pb	0.402–1.005	0.822 ± 0.220	0.01	0.21	0.0081
Cd	0.235–0.506	0.415 ± 0.100	0.003	0.033	0.0079
Zn	0.128–0.217	0.177 ± 0.031	– [c]	0.09	0.081
Mn	0.054–0.194	0.138 ± 0.054	0.08 [e]	–	–
Cu	0.058–0.117	0.088 ± 0.024	2	0.0048	0.0031

[a] WHO drinking-water guideline values [46], shown for reference only. [b] US EPA saltwater aquatic life criteria for dissolved metal, acute (CMC) and chronic (CCC) [45]. [c] No health-based guideline value. [d] No health-based guideline value; 0.3 mg L^{-1} is an acceptability threshold. [e] Provisional value.

Table 4 Exceedance factors (measured concentration divided by criterion) for metals with US EPA saltwater criteria

Metal	EF (CMC) range	EF (CMC) mean	EF (CCC) range	EF (WHO) range [a]
Pb	1.9–4.8	3.9	50–124	40–100
Cd	7.1–15.3	12.6	30–64	78–169
Zn	1.4–2.4	2.0	1.6–2.7	–
Cu	12.1–24.4	18.3	19–38	0.03–0.06

[a] For reference only; WHO guideline values apply to drinking water.

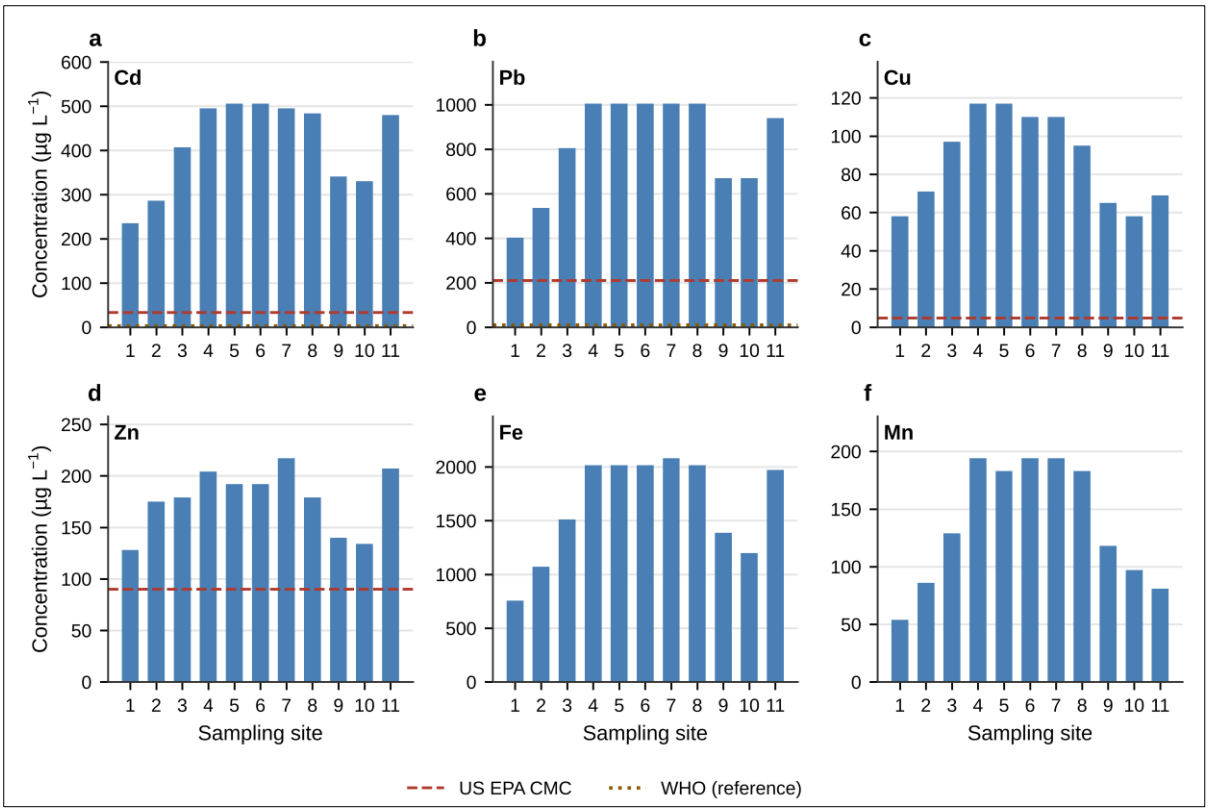


Fig. 3 Dissolved heavy metal concentrations at the 11 sampling sites. Dashed lines show the US EPA acute saltwater criterion (CMC); dotted lines show WHO drinking-water guideline values (reference only). No saltwater criteria are available for Fe and Mn

3.3 Metal–salinity relationships

All six metals increased linearly with salinity (Table 5; Fig. 4), with coefficients of determination of 0.83–0.98 ($p < 0.001$) and Spearman correlations of 0.86–0.93. Copper showed the tightest relationship ($R^2 = 0.98$) and an intercept indistinguishable from zero (1 µg L^{-1}), so that its concentration was essentially proportional to salinity. The extrapolated intercepts of Fe and Mn were slightly negative, and those of Cd, Pb and Zn were small (43–68 µg L^{-1}) compared with the measured concentrations, indicating that the low-salinity water carried much lower metal concentrations than the high-salinity water.

The departures from the regression lines were not random. For Pb, Fe, Mn and Cd, all three sites of sector A plotted below the line, by an average of 17%, 18%, 23% and 13%, respectively, whereas sites 9 and 10 in sector D plotted above it, by an average of 20%, 21%, 27% and 15%; site 8 at the northern end of sector C was also enriched (9–14%). By contrast, Cu and Zn showed no consistent departures by sector. The contrast is clearest between sites 1 and 10, which had almost identical salinities (16.3 and 15.9 psu) but differed markedly in Pb (0.402 vs

0.670 mg L^{-1}), Fe (0.756 vs 1.197), Mn (0.054 vs 0.097) and Cd (0.235 vs 0.330 mg L^{-1}), while Cu (0.058 at both) and Zn (0.128 vs 0.134 mg L^{-1}) were nearly the same.

Table 5 Ordinary least-squares regressions of dissolved metal concentrations (µg L^{-1}) on salinity (psu) and Spearman correlations with salinity (n = 10)

Metal	Slope ± SE	Intercept	R^2	p	ρ
Cd	13.7 ± 1.8	53	0.88	< 0.001	0.88
Pb	29.6 ± 4.7	43	0.83	< 0.001	0.86
Cu	3.4 ± 0.2	1	0.98	< 0.001	0.88
Zn	4.1 ± 0.5	68	0.89	< 0.001	0.93
Fe	63.8 ± 9.4	−50	0.85	< 0.001	0.88
Mn	7.0 ± 1.0	−38	0.87	< 0.001	0.92

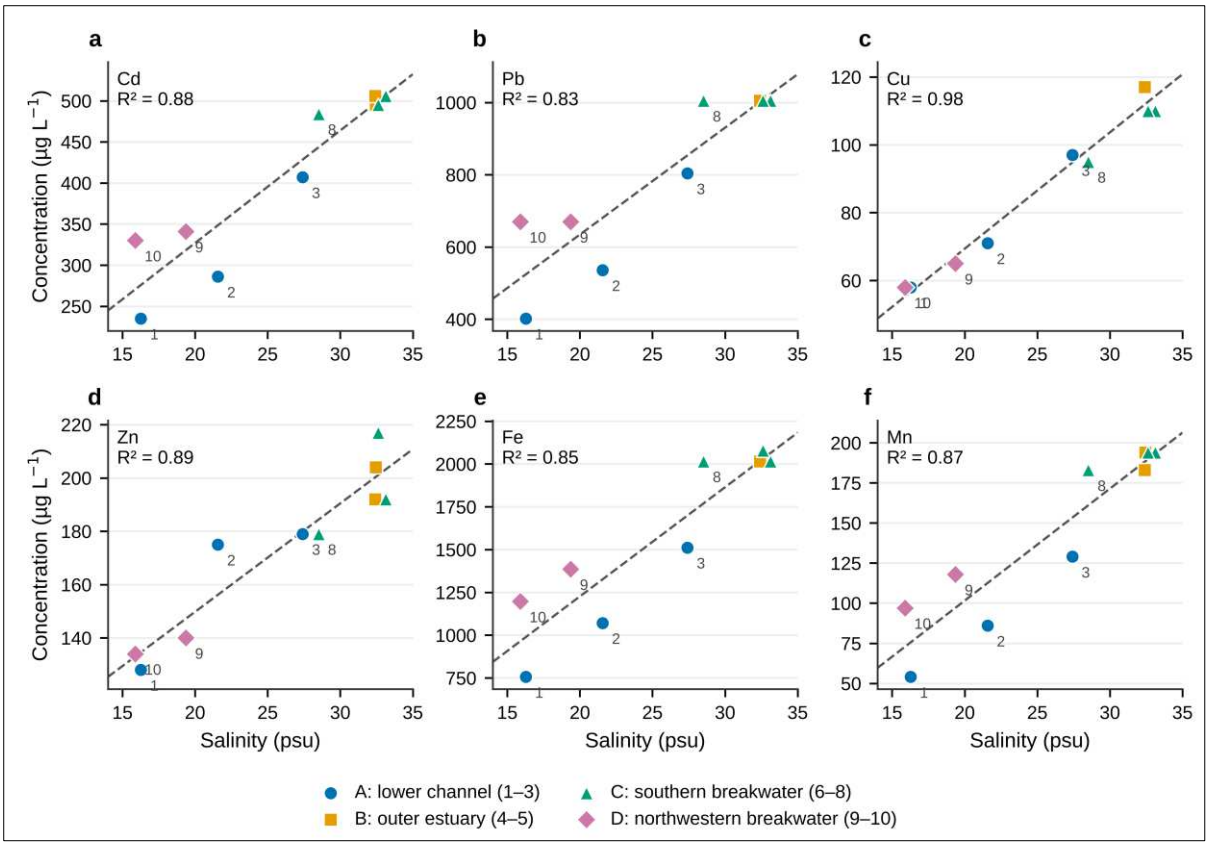


Fig. 4 Relationships between dissolved metal concentrations and salinity for (a) Cd, (b) Pb, (c) Cu, (d) Zn, (e) Fe and (f) Mn (sites 1–10). Symbols denote sectors A–D; dashed lines are ordinary least-squares regressions

3.4 Salinity-normalised metal patterns

Salinity normalisation separated the metals into two groups (Fig. 5). Normalised Cu was nearly uniform across all sites (3.3–3.7 µg L^{-1} psu^{-1}; CV 4.1%), and normalised Zn varied without a consistent spatial pattern (CV 13.6%). In contrast, normalised Pb, Fe, Mn and Cd were lowest

in sector A and increased towards sector D. Mean normalised Pb rose from 26.3 µg L^{-1} psu^{-1} in sector A to 38.4 in sector D, Fe from 50.4 to 73.5 and Cd from 14.2 to 19.2, corresponding to factors of 1.35–1.46; normalised Mn was about 1.5 times higher in sectors B–D (5.8–6.1) than in sector A (4.0). Normalised Pb, Fe, Mn and Cd were strongly inter-correlated ($\rho = 0.84$–0.95), whereas normalised Cu and Zn were not correlated with them ($|\rho| \leq 0.33$), confirming that the four metals share a common spatial signal that is independent of salinity.

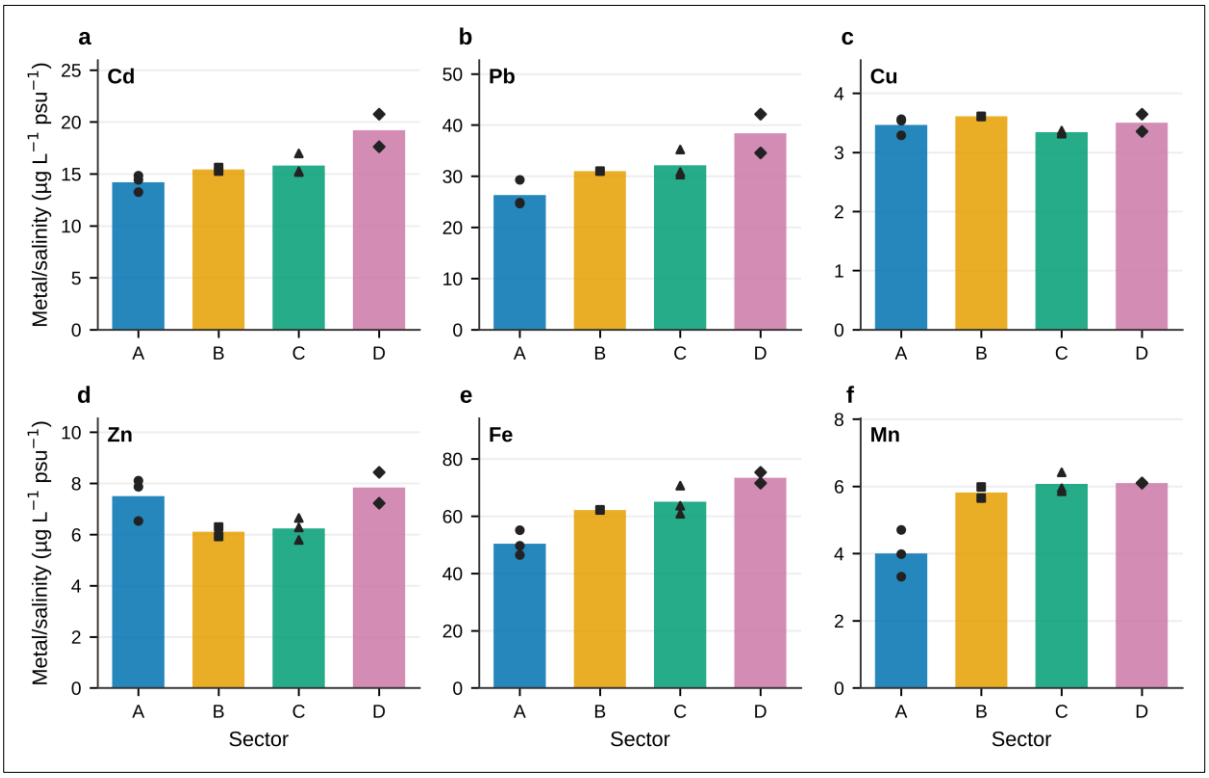


Fig. 5 Salinity-normalised concentrations (metal/salinity) of (a) Cd, (b) Pb, (c) Cu, (d) Zn, (e) Fe and (f) Mn by sector. Bars show sector means and symbols individual sites. A, lower Shatt Al-Arab channel; B, outer estuary; C, southern breakwater; D, northwestern breakwater

3.5 Spatial patterns and spectral indices

The IDW maps of the metals (Fig. 6) closely reproduced the salinity pattern, with Cd, Pb, Fe, Mn and Zn hot spots in the south-central and eastern sectors and lower values along the river channel. The NDWI map (Fig. 7a) delineated open water, the Shatt Al-Arab channel, the intertidal flats and the land–water boundary, and showed lower index values in the river channel and nearshore waters than in the open Gulf, consistent with higher suspended-sediment loads. The turbidity index (Fig. 7b) was high over the outer estuary and the extensive tidal flats east of the river mouth (around sites 4 and 5) and moderate in the open Gulf southwest of the breakwater, whereas the sheltered basin enclosed by the port breakwater (adjacent to sites 6–9) had the lowest values, indicating calm, low-turbidity water with restricted exchange.

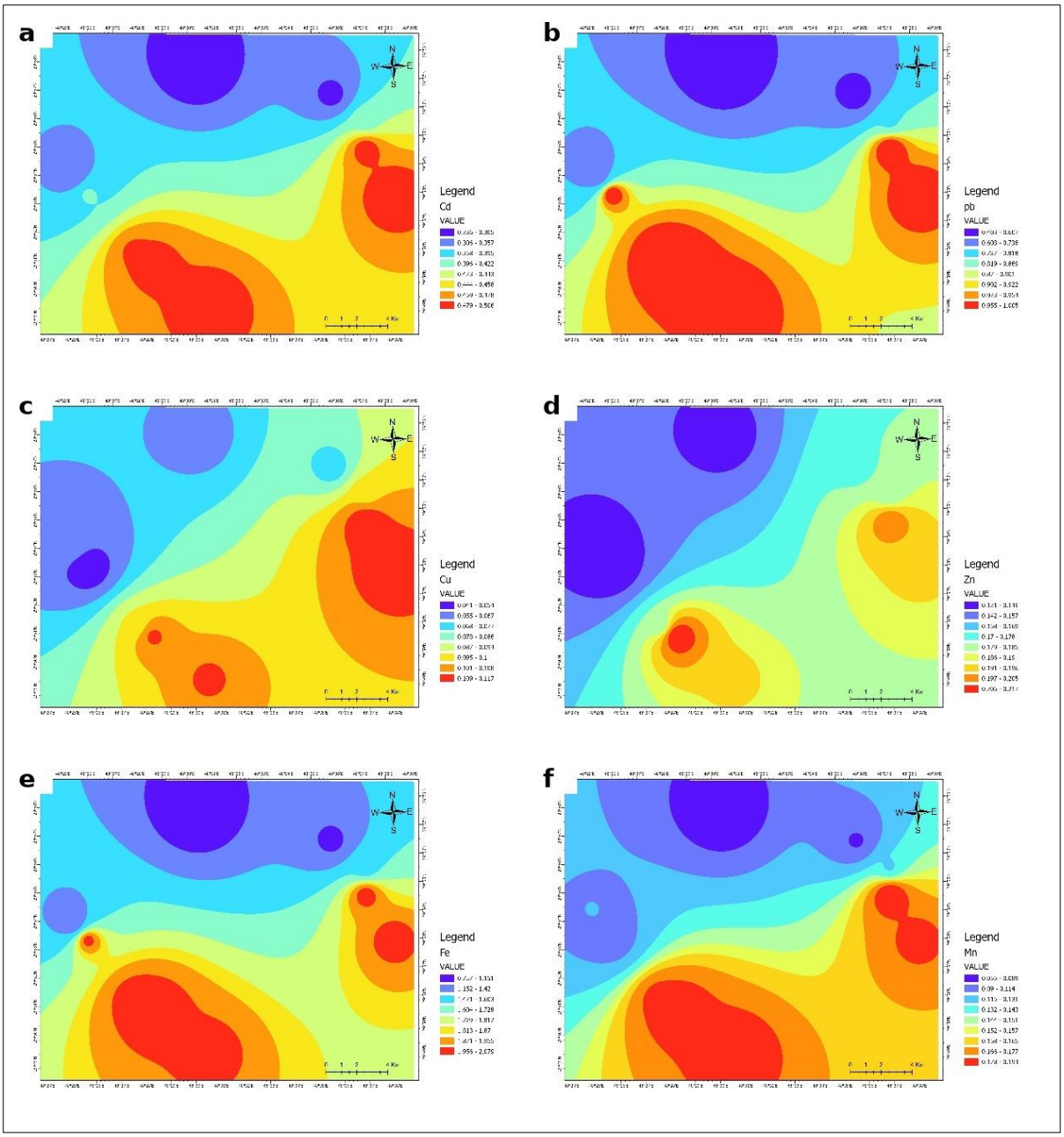


Fig. 6 IDW interpolation maps of dissolved (a) Cd, (b) Pb, (c) Cu, (d) Zn, (e) Fe and (f) Mn (mg L^{-1})

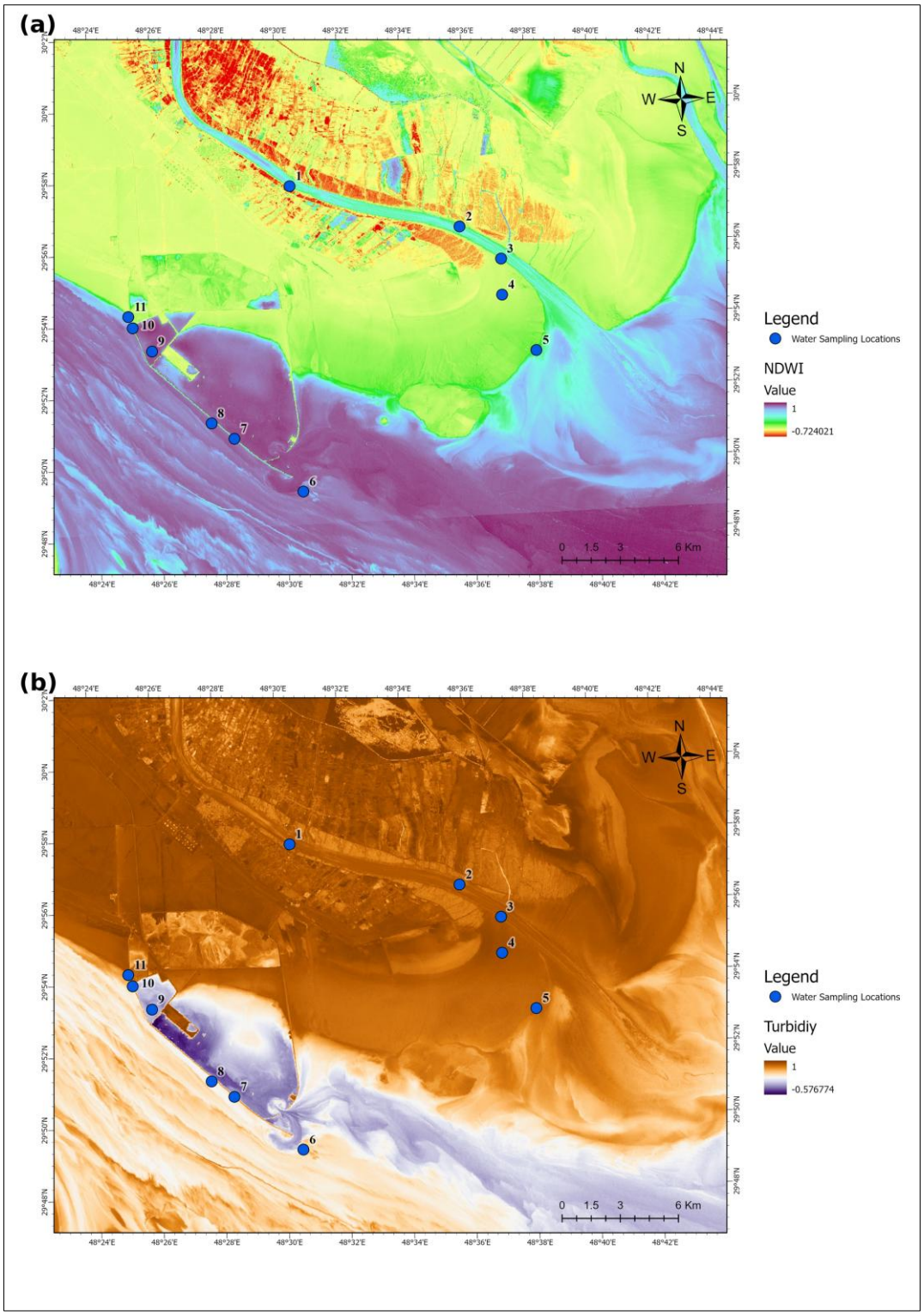


Fig. 7 Sentinel-2-derived (a) Normalized Difference Water Index (NDWI) and (b) relative turbidity index of the study area, with sampling sites

3.6 Multivariate structure

Inter-metal Spearman correlations were high ($\rho = 0.82–0.96$, $p < 0.01$), and every metal was correlated with EC ($\rho = 0.84–0.97$) and salinity ($\rho = 0.86–0.93$). Two principal components had eigenvalues above 1 and together explained 86.3% of the variance (Table 6; Fig. 8). PC1

(eigenvalue 8.28; 75.3%) had high positive loadings for all metals (0.89–0.99), EC (0.99), salinity (0.96) and DO (0.71) and represents the salinity gradient. PC2 (eigenvalue 1.20; 11.0%) was associated with water temperature (0.70) and pH (0.64). Site scores separated the least saline site 1 (PC1 = −5.1) and sites 2, 9 and 10 from the high-salinity sites 4–7 (PC1 = 2.4–2.9).

Table 6 Loadings of the retained principal components (n = 10 sites, 11 variables); loadings ≥ |0.70| in bold

Variable	PC1	PC2
Zn	**0.89**	−0.35
Cu	**0.95**	−0.20
Pb	**0.98**	0.17
Fe	**0.98**	0.15
Mn	**0.98**	0.13
Cd	**0.99**	0.11
EC	**0.99**	0.13
Salinity	**0.96**	−0.20
DO	**0.71**	−0.09
pH	0.44	0.64
Water temperature	−0.31	**0.70**
Eigenvalue	8.28	1.20
Variance (%)	75.3	11.0
Cumulative (%)	75.3	86.3

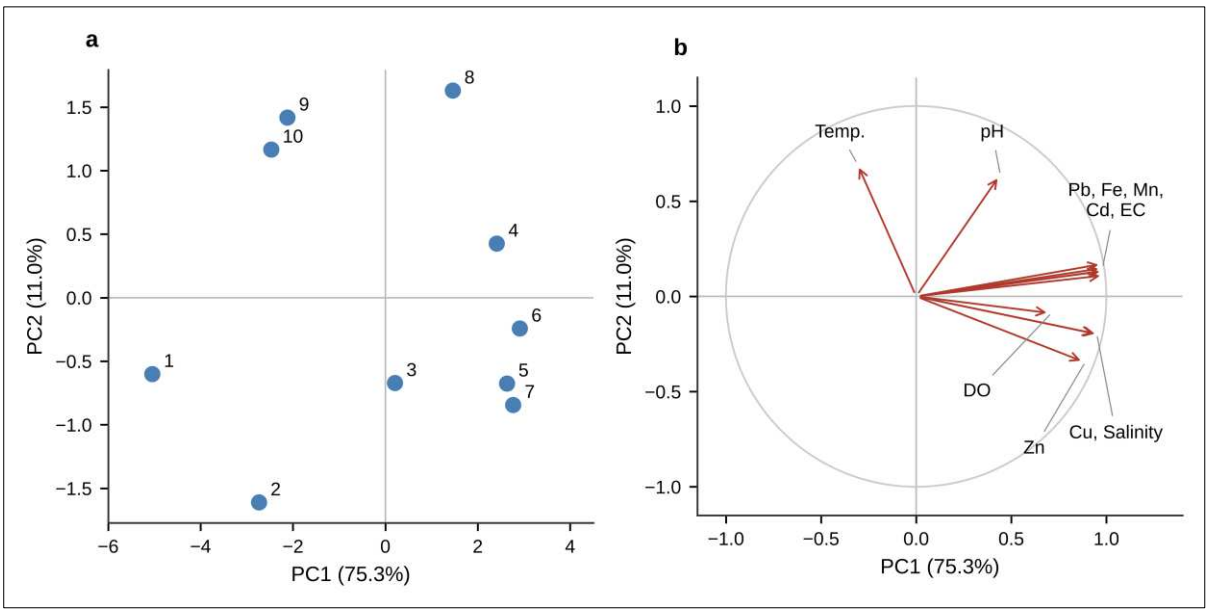


Fig. 8 Principal component analysis of physicochemical parameters and dissolved metals: (a) site scores and (b) variable loadings on PC1 and PC2

4 Discussion

4.1 The salinity gradient of the Shatt Al-Arab outlet

The seaward increase in salinity and EC, and the dominance of a single salinity-related principal component, show that mixing between Shatt Al-Arab water and Gulf water is the main control on water quality in the outlet, in agreement with the strong seasonal influence of seawater on the lower Shatt Al-Arab at Al-Faw [17, 34]. Even the least saline site in the channel (site 1), about 15–20 km upstream of the river mouth, had a salinity of 16 psu, confirming that saline water now penetrates far into the river. This agrees with the reported upstream migration of the salt front, attributed to declining river discharge, upstream water use and the tidal regime [15–17]. The low salinities at the northwestern end of the breakwater (sector D) indicate a second source of less saline water on the Khor Abdullah side, possibly agricultural drainage water delivered to the Gulf by the Main Outfall Drain through Shatt Al-Basra and Khor Al-Zubair [49], so the study area is better described as two low-salinity inputs mixing with Gulf water than as a single river–sea gradient. The low DO, including hypoxic values at sites 1, 2 and 9, is consistent with the oxygen demand of organic matter and wastewater carried by the low-salinity inputs and with low oxygen solubility at 28–30 °C, whereas the more saline, well-mixed Gulf-facing waters were better oxygenated.

4.2 Metal behaviour along the mixing gradient

The strong linear increase of all metals with salinity, with small or negative intercepts, indicates that the high-salinity water of the outer estuary and the Gulf-facing sector carried much more dissolved metal than the low-salinity inputs. This is opposite to the pattern usually observed in estuaries, where river water is the main source of dissolved metals and concentrations decrease seaward through dilution and removal [1, 50]. The regression lines therefore describe the dilution of a metal-rich, high-salinity water mass by less contaminated low-salinity water, rather than the transport of river-borne metals to the sea.

Within this overall pattern, the consistent negative departures of Pb, Fe, Mn and Cd in the river channel (sector A) indicate non-conservative behaviour. For Fe and Mn, removal at low salinity through the flocculation of colloidal oxyhydroxides and organic matter is well established [2], and particle-reactive Pb is commonly scavenged with these phases [50]. For Cd, the same concave pattern is more plausibly explained by addition at higher salinity, as increasing chloride complexation releases Cd from suspended particles [4, 5]. The near-perfect proportionality of Cu to salinity and its uniform normalised concentrations suggest that Cu

behaved conservatively along the gradient, with a single dominant source in the high-salinity water.

4.3 Local enrichment in the northwestern port sector

Salinity normalisation revealed a coherent enrichment of Pb, Fe, Mn and Cd at the northwestern end of the port breakwater (sites 9 and 10) and at site 8. At equal salinity, sites 10 and 1 differed by 40–80% in these four metals, which cannot be explained by dilution. This sector lies next to the sheltered port basin, where restricted water exchange, dredging, construction, ship traffic and fuel handling may introduce and retain metals, and close to the shipping channel of Khor Abdullah [12, 14]. Resuspension of contaminated sediments and legacy inputs from wrecks and military debris in the northern Gulf [31, 32] are additional possible sources. The low turbidity of the port basin (Fig. 7b) suggests that the enrichment is not simply due to suspended particles in the water column, although partitioning between dissolved and particulate phases can shift with salinity and particle load [7, 8]. Sediment and particulate-metal data would help to confirm the source.

4.4 Analytical considerations

The measured concentrations are within the range of some earlier studies of Iraqi marine waters that also used flame atomic absorption: Saleh et al. [35] reported Pb of 0.164–0.253 mg L^{-1} and Zn of 0.144–0.193 mg L^{-1}, and Abdulnabi [37] reported mean Pb and Cd of 0.923 and 0.052 mg L^{-1} between Al-Faw, Khor Abdullah and Khor Al-Zubair. They are much higher than those reported for the Shatt Al-Arab River itself, where dissolved metals were within permissible limits and contamination was concentrated in the bed sediments [34], and three to four orders of magnitude higher than typical dissolved concentrations in uncontaminated coastal and open-ocean waters [50]. Direct aspiration of seawater into a flame is affected by high salt loads and non-specific background absorption, which tend to raise apparent concentrations in proportion to salinity; reliable determination normally requires trace-metal-clean sampling and matrix separation or preconcentration [50]. Such a bias could produce metal–salinity proportionality like that observed for Cu, and with the present data the two explanations cannot be distinguished for Cu.

Salinity normalisation, however, provides an internal check. A bias proportional to salt content is removed by normalisation and cannot generate the sector-specific departures observed for Pb, Fe, Mn and Cd, particularly the large differences between sites of equal salinity. These spatial signals are therefore considered robust, even if the absolute concentrations are

uncertain. The identical maximum values of Pb (1.005 mg L^{-1}) and Fe (2.016 mg L^{-1}) at sites 4–8 suggest that the upper calibration limit may have been reached there; this would, if anything, underestimate concentrations in sectors B and C and does not affect the comparison between sectors A and D, where values were below this limit. The absolute concentrations and exceedance factors should accordingly be regarded as indicative until confirmed with matrix-matched calibration, a certified seawater reference material or an independent technique such as ICP-MS.

4.5 Ecological significance

Previous studies of the region have usually compared seawater with WHO drinking-water guidelines, under which Zn and Cu appear harmless. When the appropriate marine criteria are applied [45], Cu shows the largest exceedance of the acute criterion after Cd, and Zn also exceeds it at every site. Even allowing for analytical uncertainty, the combination of elevated metals, hypoxia at several sites and high summer temperatures indicates considerable stress for estuarine biota, particularly in the port sector where enrichment and restricted exchange coincide.

4.6 Hydroclimatic context

The 2014–2024 record from Al-Faw shows strong interannual variability without a significant trend (Table 7). Mean daily precipitation ranged from 0.03 mm d^{-1} (2014) to 0.89 mm d^{-1} (2018) (mean 0.41 ± 0.27 mm d^{-1}; CV 66%), and the Mann–Kendall test indicated no significant trend ($S = 17$, $Z = 1.25$, $p = 0.21$; Sen's slope +0.033 mm d^{-1} yr^{-1}). Annual mean air temperature varied between 24.26 °C (2024) and 26.78 °C (2018) (mean 25.84 ± 0.64 °C), also without a significant trend ($S = -12$, $Z = -0.86$, $p = 0.39$); the negative Sen's slope (−0.044 °C yr^{-1}) is driven by the low 2024 value. An 11-year record is too short to detect trends against this variability and does not contradict the longer-term warming of the Gulf [21] or the drying projected for Iraq [19, 22]. Because local rainfall is negligible in absolute terms, the main hydroclimatic control on the outlet is the reduced Tigris–Euphrates inflow combined with high evaporation, which strengthens the Gulf-derived salinity signal and lengthens residence times [16, 17]. Under these conditions, the high-salinity, metal-rich water identified here is likely to extend further into the estuary, while warming and declining oxygen can increase metal bioavailability and toxicity [6–8].

Table 7 Annual mean daily precipitation and mean air temperature at the Al-Faw station, 2014–2024, with trend statistics

Year	Precipitation (mm d^{-1}) [a]	Air temperature (°C)
2014	0.03	26.00
2015	0.53	25.72
2016	0.21	25.97
2017	0.13	26.18
2018	0.89	26.78
2019	0.39	25.65
2020	0.66	25.50
2021	0.15	26.33
2022	0.28	26.18
2023	0.57	25.71
2024	0.64	24.26
Mean ± SD	0.41 ± 0.27	25.84 ± 0.64
CV (%)	66	2.5
Mann–Kendall S (Z; p)	17 (1.25; 0.21)	−12 (−0.86; 0.39)
Sen's slope (per year)	+0.033	−0.044

[a] **Precipitation unit: mm d^{-1}. Source: Agricultural Meteorology Centre, Ministry of Agriculture, Basra Governorate, Iraq.**

4.7 Limitations and the role of GIS and remote sensing

The combination of IDW maps and Sentinel-2 indices gave a coherent picture of the salinity gradient and of the contrast between the turbid outer estuary and the sheltered port basin. NDWI is effective for delineating water bodies and the intertidal zone [39], and red-band indices are sensitive to suspended particulate matter in turbid coastal waters [40, 41]. Several limitations should be acknowledged. The data represent a single sampling period at a small number of sites, so sector comparisons are descriptive. IDW surfaces based on eleven irregularly distributed sites extrapolate across land and tidal flats and should be read only as broad gradients. The turbidity index was not calibrated against in situ measurements, and the satellite scene and field sampling were not necessarily simultaneous. Finally, the major-ion data did not pass the charge-balance check and could not be re-analysed. Future work should combine seasonal sampling along the full salinity gradient, trace-metal-clean analysis, dissolved and particulate phases, sediments and calibrated multi-temporal remote sensing.

5 Conclusions

This study examined dissolved heavy metals along the salinity gradient of the Shatt Al-Arab outlet. The main conclusions are as follows.

- Salinity increased from 15.9 psu in the lower river channel to 33.1 psu in the Gulf-facing sector, confirming that saline water penetrates far into the Shatt Al-Arab; a second low-salinity input occurs on the Khor Abdullah side of the port breakwater.
- Dissolved oxygen was low (1.1–4.7 mg L^{-1}), with hypoxic conditions at three sites.
- All six metals increased linearly with salinity (R^2 = 0.83–0.98), indicating that the high-salinity water carried more dissolved metal than the low-salinity inputs.
- Salinity normalisation showed that Cu behaved conservatively, whereas Pb, Fe, Mn and Cd were depleted by 13–23% in the low-salinity river channel and enriched by 15–27% at the northwestern port breakwater, indicating removal during mixing and a local source, respectively.
- Cd, Pb, Cu and Zn exceeded US EPA acute saltwater criteria at all sites; Cu and Zn, which appear acceptable under drinking-water guidelines, are of concern for marine life.
- Because a salt-matrix bias would scale with salinity, salinity-normalised data provide a robust way to identify spatial signals when absolute concentrations from direct flame analysis are uncertain.

A seasonally resolved monitoring programme with trace-metal-clean analysis, particulate and sediment sampling and calibrated remote sensing is recommended, with priority given to the port sector.

Declarations

Author contributions: A.A.A.-H.: fieldwork, laboratory analysis, writing original draft; M.M.M.: conceptualization, supervision, GIS and remote sensing analysis, writing review and editing; G.K.J.: fieldwork, data curation, visualization, H. B. G. conceptualization, writing review, statistical analysis and editing. All authors read and approved the final manuscript.

Funding The authors declare that no funds, grants or other support were received during the preparation of this manuscript.

Data Availability: The hydrochemical data used in this study were generated through laboratory analyses of water samples collected and analyzed by the authors. All data generated and analyzed during this study are included in the article and its supplementary information (ESM 1). Sentinel-2 satellite imagery is freely available through the Copernicus Data Space Ecosystem.

Ethics approval and consent to participate Not applicable.

Consent for publication: Not applicable.

Competing Interests: Hussein B. Ghalib is an Editorial Board Member of Discover Geoscience and confirms that he was not involved in the handling or decision-making of this manuscript. The remaining authors declare that they have no competing interests.

References

1. Boyle EA, Collier R, Dengler AT, Edmond JM, Ng AC, Stallard RF. On the chemical mass-balance in estuaries. Geochim Cosmochim Acta. 1974;38(11):1719–28. https://doi.org/10.1016/0016-7037(74)90188-4
2. Sholkovitz ER. Flocculation of dissolved organic and inorganic matter during the mixing of river water and seawater. Geochim Cosmochim Acta. 1976;40(7):831–45. https://doi.org/10.1016/0016-7037(76)90035-1
3. Officer CB. Discussion of the behaviour of nonconservative dissolved constituents in estuaries. Estuar Coast Mar Sci. 1979;9(1):91–4. https://doi.org/10.1016/0302-3524(79)90009-4

4. Elbaz-Poulichet F, Martin JM, Huang WW, Zhu JX. Dissolved Cd behaviour in some selected French and Chinese estuaries: consequences on Cd supply to the ocean. Mar Chem. 1987;22(2–4):125–36. https://doi.org/10.1016/0304-4203(87)90004-1

5. Comans RNJ, van Dijk CPJ. Role of complexation processes in cadmium mobilization during estuarine mixing. Nature. 1988;336:151–4. https://doi.org/10.1038/336151a0

6. Hoffmann LJ, Breitbarth E, Boyd PW, Hunter KA. Influence of ocean warming and acidification on trace metal biogeochemistry. Mar Ecol Prog Ser. 2012;470:191–205. https://doi.org/10.3354/meps10082

7. Hatje V, Sarin M, Sander SG, Omanović D, Ramachandran P, Völker C, et al. Emergent interactive effects of climate change and contaminants in coastal and ocean ecosystems. Front Mar Sci. 2022;9:936109. https://doi.org/10.3389/fmars.2022.936109

8. Zitoun R, Marcinek S, Hatje V, Sander SG, Völker C, Sarin M, Omanović D. Climate change driven effects on transport, fate and biogeochemistry of trace element contaminants in coastal marine ecosystems. Commun Earth Environ. 2024;5. https://doi.org/10.1038/s43247-024-01679-y

9. Reynolds RM. Physical oceanography of the Gulf, Strait of Hormuz, and the Gulf of Oman results from the Mt Mitchell expedition. Mar Pollut Bull. 1993;27:35–59. https://doi.org/10.1016/0025-326X(93)90007-7

10. Al-Yamani F. Importance of the freshwater influx from the Shatt-Al-Arab River on the Gulf marine environment. In: Abuzinada AH, Barth HJ, Krupp F, Böer B, Al Abdessalaam TZ, editors. Protecting the Gulf's marine ecosystems from pollution. Basel: Birkhäuser; 2008. p. 207–22. https://doi.org/10.1007/978-3-7643-7947-6_11

11. Alosairi Y, Alsulaiman N, Petrov P, Karam Q. Responses of salinity and chlorophyll-a to extreme rainfall events in the northwest Arabian Gulf: emphasis on Shatt Al-Arab. Mar Pollut Bull. 2019;149:110564. https://doi.org/10.1016/j.marpolbul.2019.110564

12. Sheppard C, Al-Husiani M, Al-Jamali F, Al-Yamani F, Baldwin R, Bishop J, et al. The Gulf: a young sea in decline. Mar Pollut Bull. 2010;60(1):13–38. https://doi.org/10.1016/j.marpolbul.2009.10.017

13. Vaughan GO, Al-Mansoori N, Burt JA. The Arabian Gulf. In: Sheppard C, editor. World seas: an environmental evaluation. 2nd ed. Vol. 2. London: Academic Press; 2019. https://doi.org/10.1016/B978-0-08-100853-9.00001-4

14. Hosseini H, Saadaoui I, Moheimani N, Al Saidi M, Al Jamali F, Al Jabri H, Ben Hamadou R. Marine health of the Arabian Gulf: drivers of pollution and assessment approaches focusing on desalination activities. Mar Pollut Bull. 2021;164:112085. https://doi.org/10.1016/j.marpolbul.2021.112085

15. Hameed HA, Ali MH, Aljorany YS, Hassan WF, Alhello AA. Assessing changes in seawater intrusion and water quality of the Shatt Al-Arab River, Iraq. Ann Limnol Int J Limnol. 2013;49(3):199–206. https://doi.org/10.1051/limn/2013054

16. Abdullah AD, Karim UFA, Masih I, Popescu I, van der Zaag P. Anthropogenic and tidal influences on salinity levels of the Shatt al-Arab River, Basra, Iraq. Int J River Basin Manag. 2016;14(3):357–66. https://doi.org/10.1080/15715124.2016.1193509

17. Al-Asadi SAR, Alhello AA, Ghalib HB, Muttashar WR, Al-Eydawi HT. Seawater intrusion into Shatt Al-Arab River, northwest Arabian/Persian Gulf. J Appl Water Eng Res. 2022. https://doi.org/10.1080/23249676.2022.2113460

18. Al-Qurnawi WS, Ghalib HB, Al-Abadi MAA, Al Hawash AB. Corrosion–scaling potentiality of domestic water pipelines and evaluation of the applicability of raw water sources in Basrah, Iraq. Iraqi J Sci. 2022;63(5):2089–102. https://doi.org/10.24996/ijs.2022.63.5.24

19. Adamo N, Al-Ansari N, Sissakian VK, Knutsson S, Laue J. Climate change: consequences on Iraq's environment. J Earth Sci Geotech Eng. 2018;8(3):43–58.

20. Awadh SM, Al-Dabbas M. Location, physiography, and atmospheric hazards. In: The geography of Iraq. Cham: Springer Nature Switzerland; 2024. p. 1–18.

21. Al Senafi F, Al Rushaid T, Al Mukaimi M. Climate variability of air temperature and its warming trends in the Arabian Gulf. Earth Syst Environ. 2024;8(3):587–98. https://doi.org/10.1007/s41748-024-00395-z

22. IPCC. Climate change 2021: the physical science basis. Contribution of Working Group I to the Sixth Assessment Report of the Intergovernmental Panel on Climate Change. Cambridge: Cambridge University Press; 2021. https://doi.org/10.1017/9781009157896

23. Mahdi MM, Ismail MJ, Mohammad OA. The integration of wireline logs and sedimentological data to predict sequence stratigraphic framework in carbonate rocks: an example from Rumaila Formation (Cenomanian), West Qurna Oil Field, southern Iraq. Stratigr Geol Correl. 2022;30(5):360–77. https://doi.org/10.1134/S0869593822050045

24. Lazim AA, Ismail MJ, Mahdi MM. High-resolution sequence stratigraphy of the Mishrif Formation (Cenomanian–Early Turonian) at Zubair Oilfield (Al-Rafdhiah dome), southern Iraq. Petrol Res. 2024;9(1):61–71. https://doi.org/10.1016/j.ptlrs.2023.08.002

25. Al-Qadir SA, Al-Ali AK, Soltan BH. Monitoring soil contamination by hydrocarbons and heavy metals in parts of Basra, southern Iraq, using remote sensing and GIS techniques. Iraqi Geol J. 2023;56(1D):29–42. https://doi.org/10.46717/igj.56.1D.3ms-2023-4-12

26. Saleem FM, Al-Hejuje MM, Al-Saad HT. Concentrations, sources and distribution of polycyclic aromatic hydrocarbon (PAHs) compounds in Basrah soils, Iraq. Baghdad Sci J. 2023;20(3):755–69. https://doi.org/10.21123/bsj.2022.6979

27. Resen MA, Abdulhassan HK, Al-Saad HT. Total petroleum hydrocarbons in soil of different oil fields at Basrah Governorate, Iraq. Vet Med Public Health J. 2024;5(2):158–65. https://doi.org/10.31559/VMPH2024.5.2.17

28. Kareem I, Taher M, Ali A, Hassan HA, Nasser F, Na'ma M, et al. Evaluating the environmental impact of industrial activities on soil in Basrah City, southern Iraq. Iraqi Geol J. 2025;58(1F):213–22. https://doi.org/10.46717/igj.2025.58.1F.15

29. Readman JW, Fowler SW, Villeneuve JP, Cattini C, Oregioni B, Mee LD. Oil and combustion-product contamination of the Gulf marine environment following the war. Nature. 1992;358:662–5. https://doi.org/10.1038/358662a0

30. Literathy P. Considerations for the assessment of environmental consequences of the 1991 Gulf War. Mar Pollut Bull. 1993;27:349–56. https://doi.org/10.1016/0025-326X(93)90042-I

31. United Nations Environment Programme. Environment in Iraq: UNEP progress report. Geneva: UNEP; 2003.

32. Al-Imarah FJM, Al-Saad HT. Oil pollution in the Shatt Al-Arab River and its estuary, 1980–2018. In: Jawad LA, editor. Tigris and Euphrates Rivers: their environment from headwaters to mouth. Cham: Springer; 2021. p. 285–97.

33. Al-Asadi SAR, Al Hawash AB, Alkhlifa NAH, Ghalib HB. Factors affecting the levels of toxic metals in the Shatt Al-Arab River, southern Iraq. Earth Syst Environ. 2019;3(2):313–25. https://doi.org/10.1007/s41748-019-00096-y

34. Al-Asadi SAR, Al-Qurnawi WS, Al Hawash AB, Ghalib HB, Alkhlifa NAH. Water quality and impacting factors on heavy metals levels in Shatt Al-Arab River, Basra, Iraq. Appl Water Sci. 2020;10(5):103. https://doi.org/10.1007/s13201-020-01196-1

35. Saleh SM, Abdulnabi ZA, Mizhir AA, Hantoush AA, Hassan WF, Al-Khion DD. Evaluation of levels of some heavy metals in marine environment, southern Iraq. Mesopot J Mar Sci. 2021;36(2). https://doi.org/10.58629/mjms.v36i2.250

36. Abdulaziz A. Changes in some of heavy elements concentrations and their relationship with some environmental factors in the Iraqi coastal water. Basrah J Sci. 2021. https://doi.org/10.29072/basjs.2021313

37. Abdulnabi ZA. Assessment of some toxic elements levels in Iraqi marine water. Mesopot J Mar Sci. 2022. https://doi.org/10.58629/mjms.v31i1.112

38. Sarasiab AR, Hosseini M, Mirsalari Z. Mercury distribution in contaminated surface sediments from four estuaries, Khuzestan shore, northern part of the Persian Gulf. Bull Environ Contam Toxicol. 2014;93:522–5. https://doi.org/10.1007/s00128-014-1354-y

39. McFeeters SK. The use of the Normalized Difference Water Index (NDWI) in the delineation of open water features. Int J Remote Sens. 1996;17(7):1425–32. https://doi.org/10.1080/01431169608948714

40. Doxaran D, Froidefond JM, Lavender S, Castaing P. Spectral signature of highly turbid waters: application with SPOT data to quantify suspended particulate matter concentrations. Remote Sens Environ. 2002;81(1):149–61. https://doi.org/10.1016/S0034-4257(01)00341-8

41. Dogliotti AI, Ruddick KG, Nechad B, Doxaran D, Knaeps E. A single algorithm to retrieve turbidity from remotely-sensed data in all coastal and estuarine waters. Remote Sens Environ. 2015;156:157–68. https://doi.org/10.1016/j.rse.2014.09.020

42. APHA, AWWA, WEF. Standard methods for the examination of water and wastewater. 23rd ed. Washington, DC: American Public Health Association; 2017.

43. Millero FJ, Feistel R, Wright DG, McDougall TJ. The composition of Standard Seawater and the definition of the Reference-Composition Salinity Scale. Deep Sea Res Part I. 2008;55(1):50–72. https://doi.org/10.1016/j.dsr.2007.10.001

44. Lu GY, Wong DW. An adaptive inverse-distance weighting spatial interpolation technique. Comput Geosci. 2008;34(9):1044–55. https://doi.org/10.1016/j.cageo.2007.07.010

45. US Environmental Protection Agency. National recommended water quality criteria – aquatic life criteria table. Washington, DC: US EPA; 2024. https://www.epa.gov/wqc/national-recommended-water-quality-criteria-aquatic-life-criteria-table. Accessed 5 Oct 2026.

46. World Health Organization. Guidelines for drinking-water quality: fourth edition incorporating the first and second addenda. Geneva: WHO; 2022.

47. Mann HB. Nonparametric tests against trend. Econometrica. 1945;13(3):245–59. https://doi.org/10.2307/1907187

48. Sen PK. Estimates of the regression coefficient based on Kendall's tau. J Am Stat Assoc. 1968;63(324):1379–89. https://doi.org/10.1080/01621459.1968.10480934

49. Asd WH, Ghalib HB, Al-Zubaydi JH. Hydrochemical study of the southern sector of the Al-Massab Al-Aam canal water, southern Iraq. Iraqi J Sci. 2022;63(8):3447–59. https://doi.org/10.24996/ijs.2022.63.8.20

50. Bruland KW, Middag R, Lohan MC. Controls of trace metals in seawater. In: Holland HD, Turekian KK, editors. Treatise on geochemistry. 2nd ed. Vol. 8. Oxford: Elsevier; 2014. p. 19–51. https://doi.org/10.1016/B978-0-08-095975-7.00602-1

Supplementary information

ESM 1 (ESM_1.xlsx) Measured field parameters, dissolved heavy metals and major ions at the 11 sampling sites, with the charge-balance errors and molar ion ratios used to assess the major-ion data, and the 2014–2024 hydroclimatic data

Supplementary Files

This is a list of supplementary files associated with this preprint. Click to download.

- ESM1.xlsx